

Supporting Information

Light-Ferroelectric Interaction in Two-Dimensional Lead Iodide Perovskites

Dohyung Kim¹, Anton V. Ievlev², Olga S. Ovchinnikova³, Sergei V. Kalinin², Mahshid
Ahmadi^{1*}

¹*Institute for Advanced Materials and Manufacturing, Department of Materials Science and
Engineering, University of Tennessee, Knoxville, TN 37996, USA*

²*Center for Nanophase Materials Sciences, Oak Ridge National Laboratory, Oak Ridge, TN
37830, United States, USA*

³*Computational Science and Engineering Division, Oak Ridge National Laboratory, Oak
Ridge, TN 37830, United States, USA*

*Corresponding authors' email: mahmadi3@utk.edu

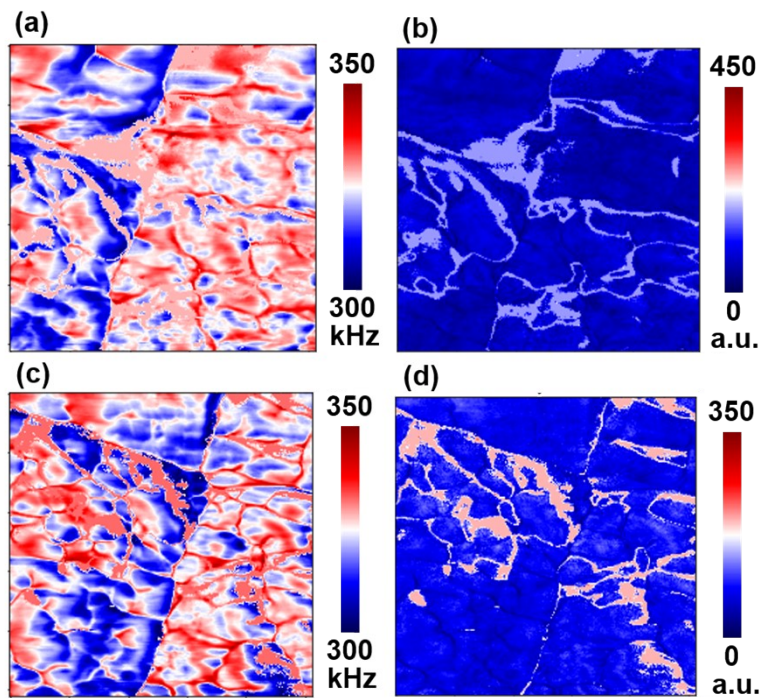


Figure S1. (a) BE-PFM frequency and (b) Q-factor maps in dark and (c-d) under illumination.

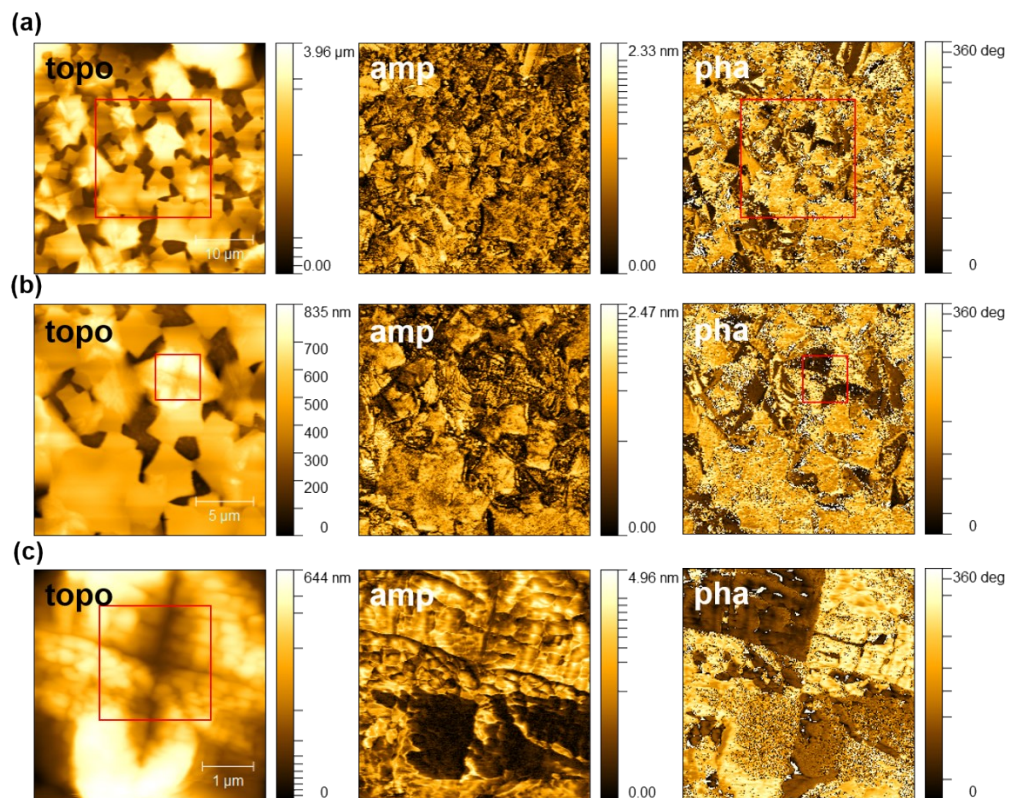


Figure S2. PFM images of the (4,4-DFPD)₂PbI₄ thin film (a) over an area of 40 μm², (b) 20 μm², and (c) 4 μm² in dark. The red boxes represent the selected areas for high-resolution PFM scans.

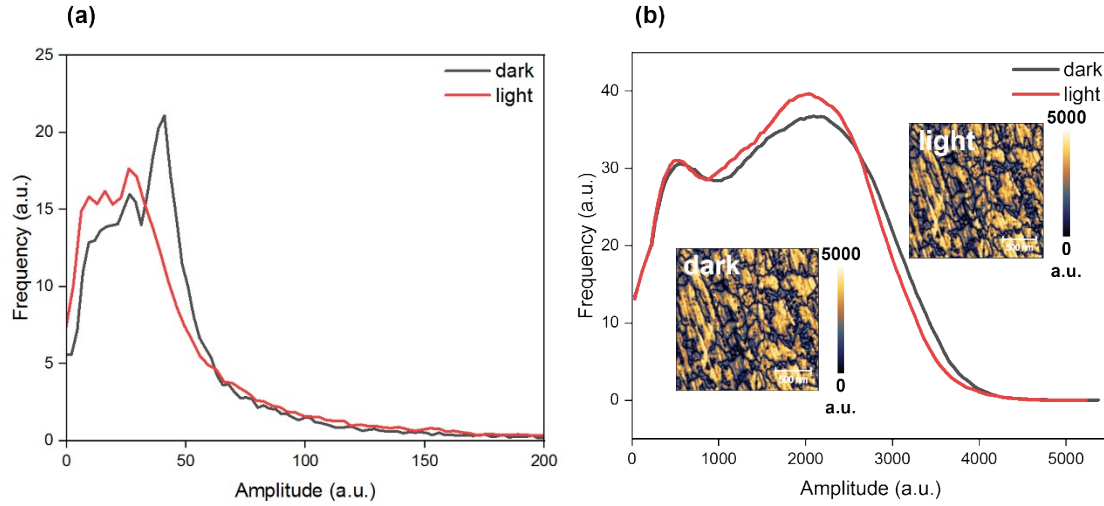


Figure S3. Histogram plot of PFM amplitude responses on (a) the (4,4-DFPD)₂PbI₄ and (b) the PLZT thin films in dark and under illumination. The insets in (b) present the PFM amplitude images in dark and under illumination.

Supplementary Note 1

To clarify the difference in amplitude responses between dark and illumination conditions, we have plotted the histogram of the amplitude responses in Figure S3a. We also have performed the PFM measurements in dark and under illumination on a standard ferroelectric sample, a lead lanthanum zirconate titanate (PLZT) thin film (see Figure S3b), to ensure our sample response is not a measurement artifact. The slight difference in amplitude response between dark and illumination in PLZT film could be possibly from shifting contact resonance frequency which is commonly observed in PFM measurements. Thus, although there is an insignificant difference in the amplitude responses in (4,4-DFPD)₂PbI₄ film between the two conditions, such difference can be neglected, especially when we consider much lower amplitude responses in (4,4-DFPD)₂PbI₄ film as compared to PLZT film.

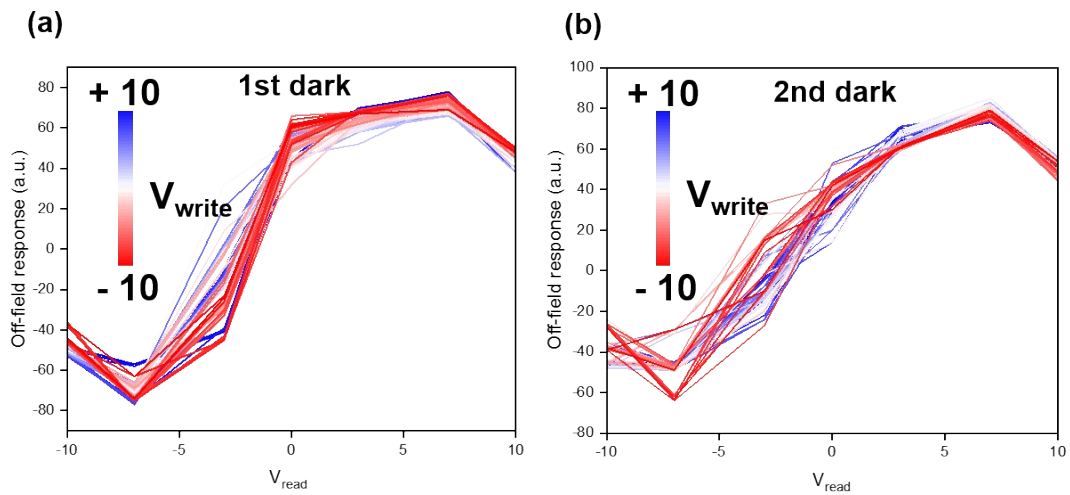


Figure S4. Averaged cKPFM curves from the (a) 1st and (b) 2nd measurements at the same region in dark.

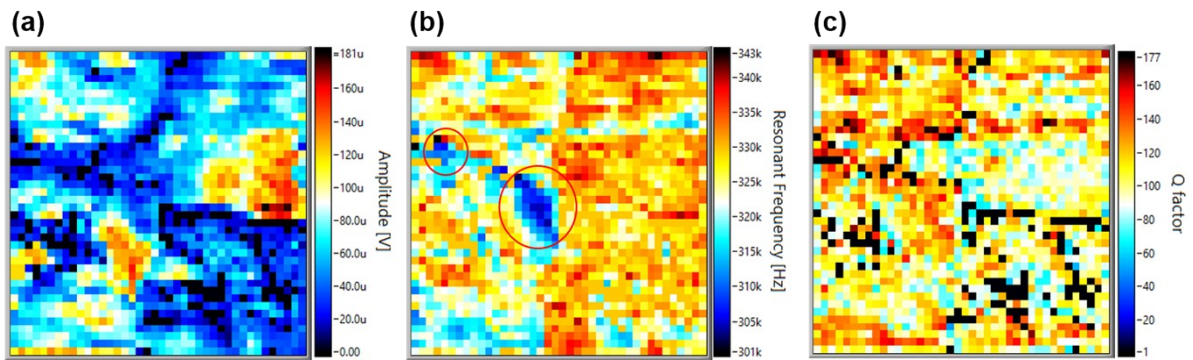


Figure S5. The loading maps of (a) amplitude, (b) frequency, and Q-factor (c) in cKPFM measurements in dark. The circles in (b) represent significantly shifted contact resonance frequency due to larger topological variations.

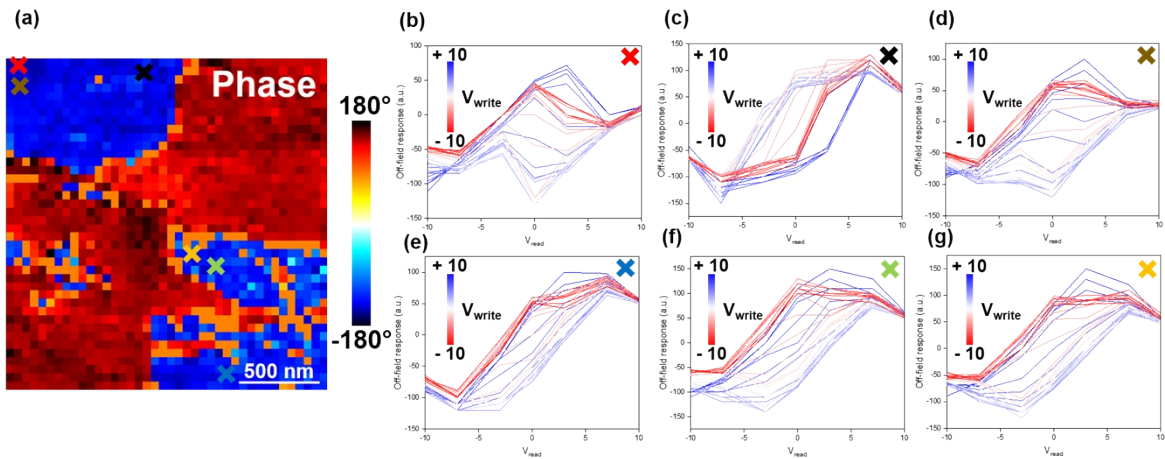


Figure S6. (a) The loading map of phase responses in cKPFM measurements in dark. Individual cKPFM curves at the '×' marked in (b) red, (c) black, (d) light-brown, (e) light-blue, (f) light-green, and (g) yellow in (a).

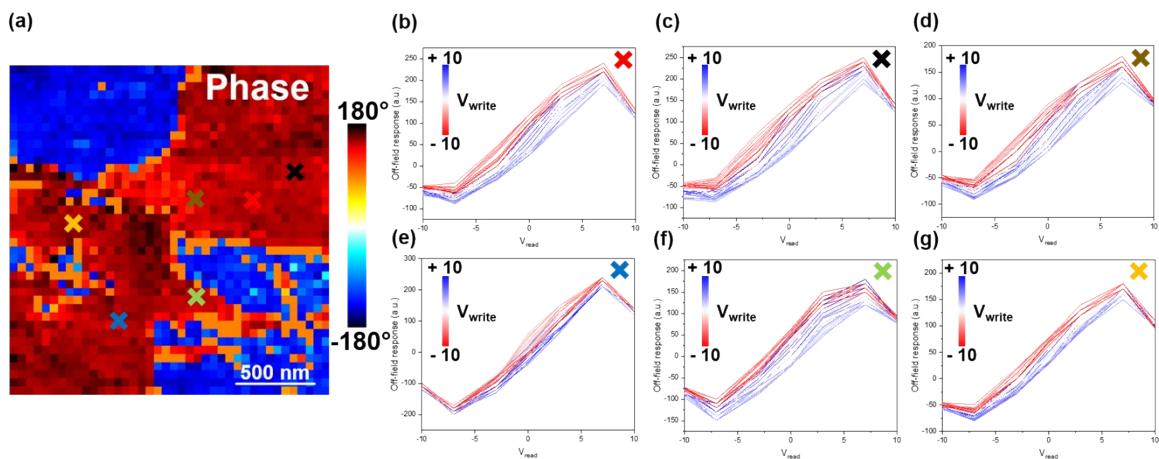


Figure S7. (a) The loading map of phase responses in cKPFM measurements in dark. Individual cKPFM curves at the '×' marked in (b) red, (c) black, (d) light-brown, (e) light-blue, (f) light-green, and (g) yellow in (a).

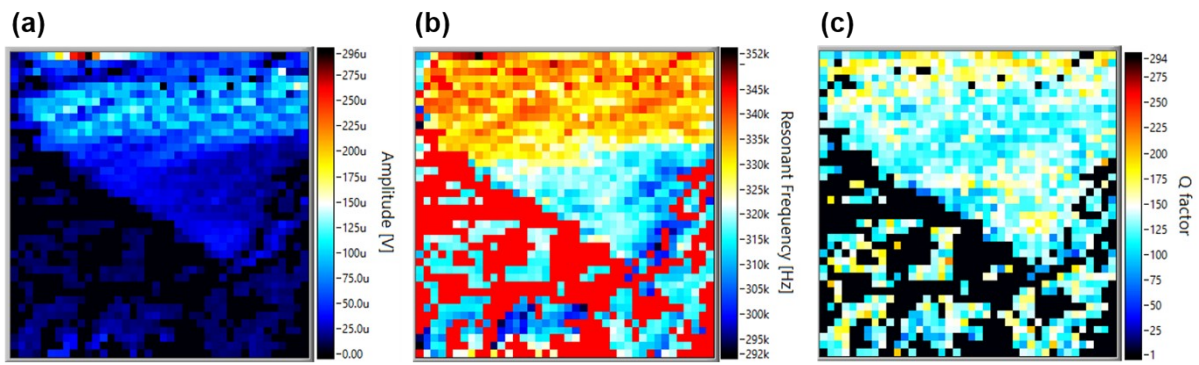


Figure S8. The loading maps of (a) amplitude, (b) frequency, and Q-factor (c) in cKPFM measurements under illumination.

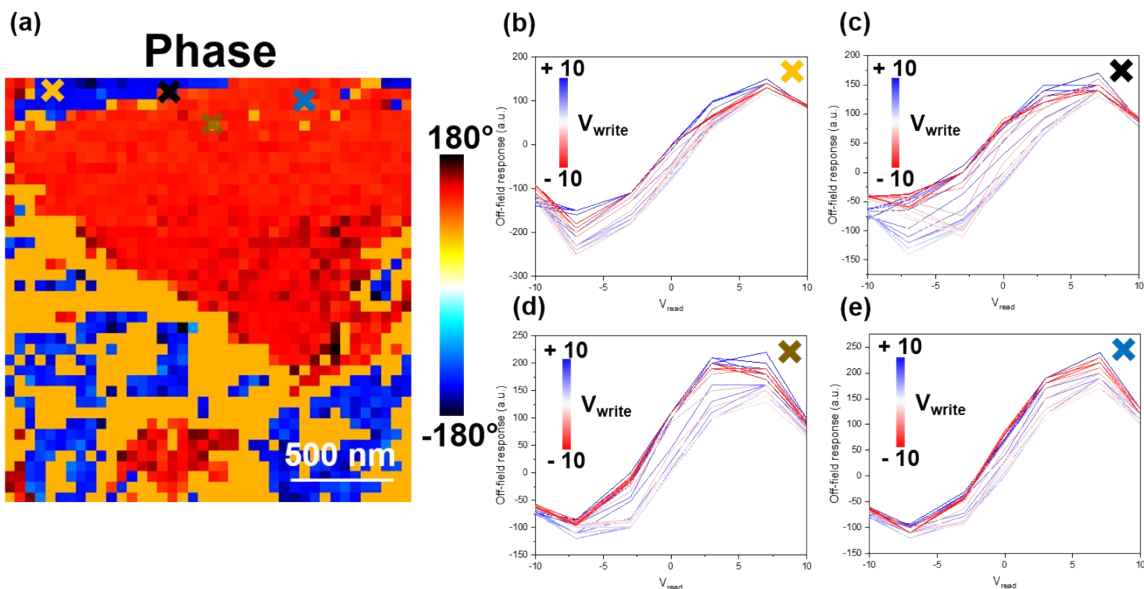


Figure S9. (a) The loading map of phase responses in cKPFM measurements under illumination. Individual cKPFM curves at the 'x' marked in (b) yellow, (c) black, (d) light-brown, and (e) light-blue in (a).

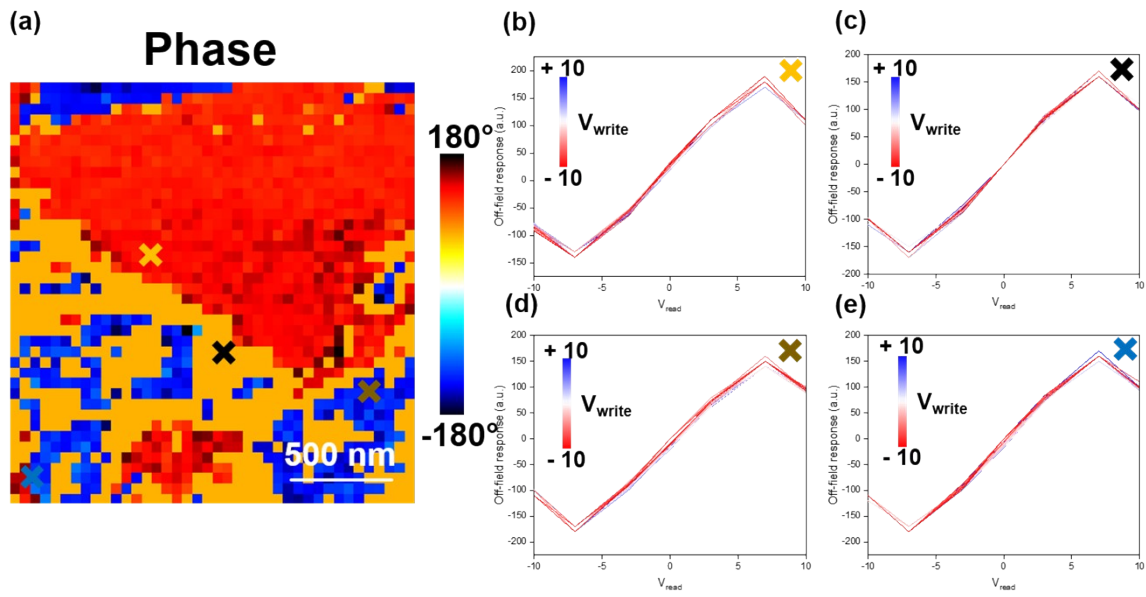


Figure S10. (a) The loading map of phase responses in cKPFM measurements under illumination. Individual cKPFM curves at the ‘x’ marked in (b) yellow, (c) black, (d) light-brown, and (e) light-blue in (a).

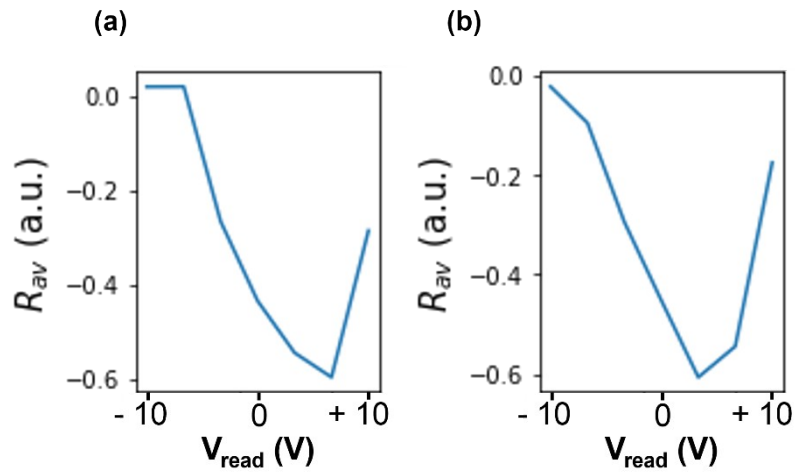


Figure S11. The 1st PCA component (a) in dark and (b) under illumination

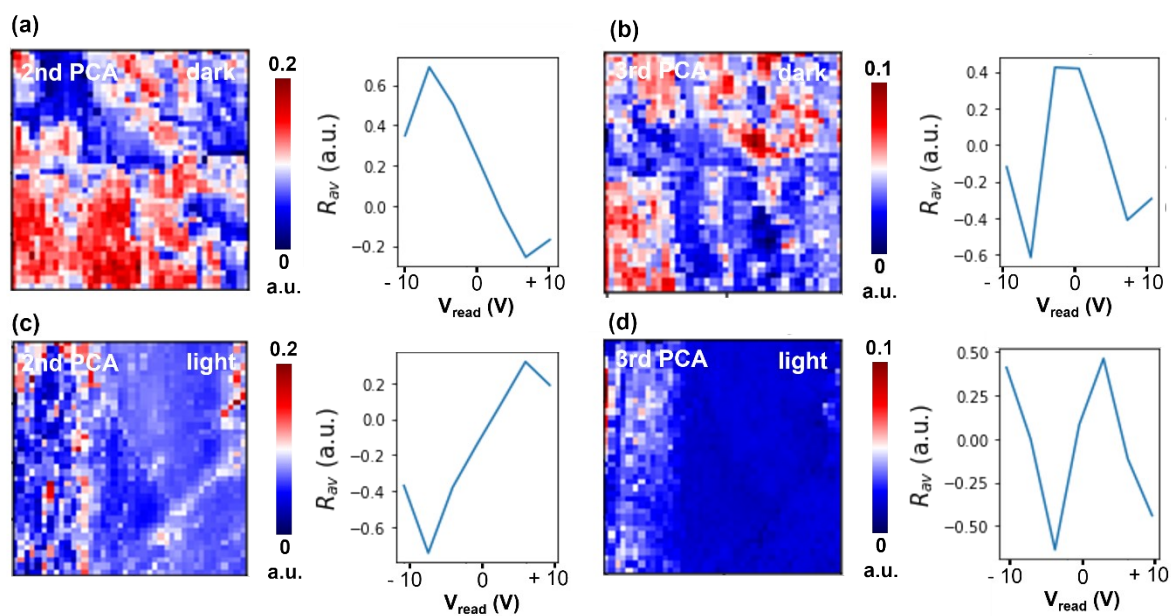


Figure S12. The 2nd and 3rd PCA components of mean deviation from cKPFM data (a-b) in dark and (c-d) under illumination.

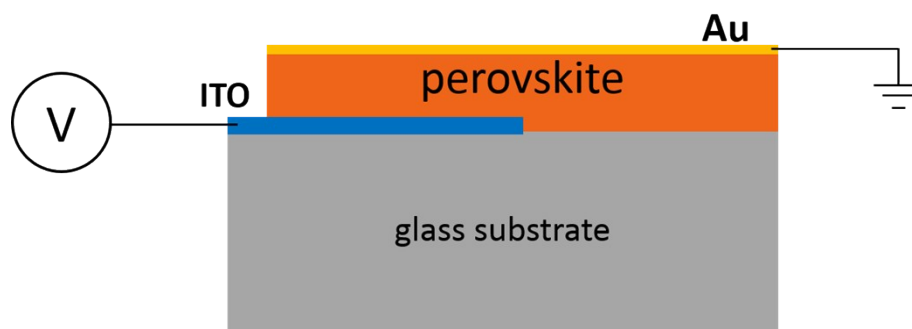


Figure S13. Schematic illustration of a planar electrode design for in-situ XRD and FORC-I-t measurements.

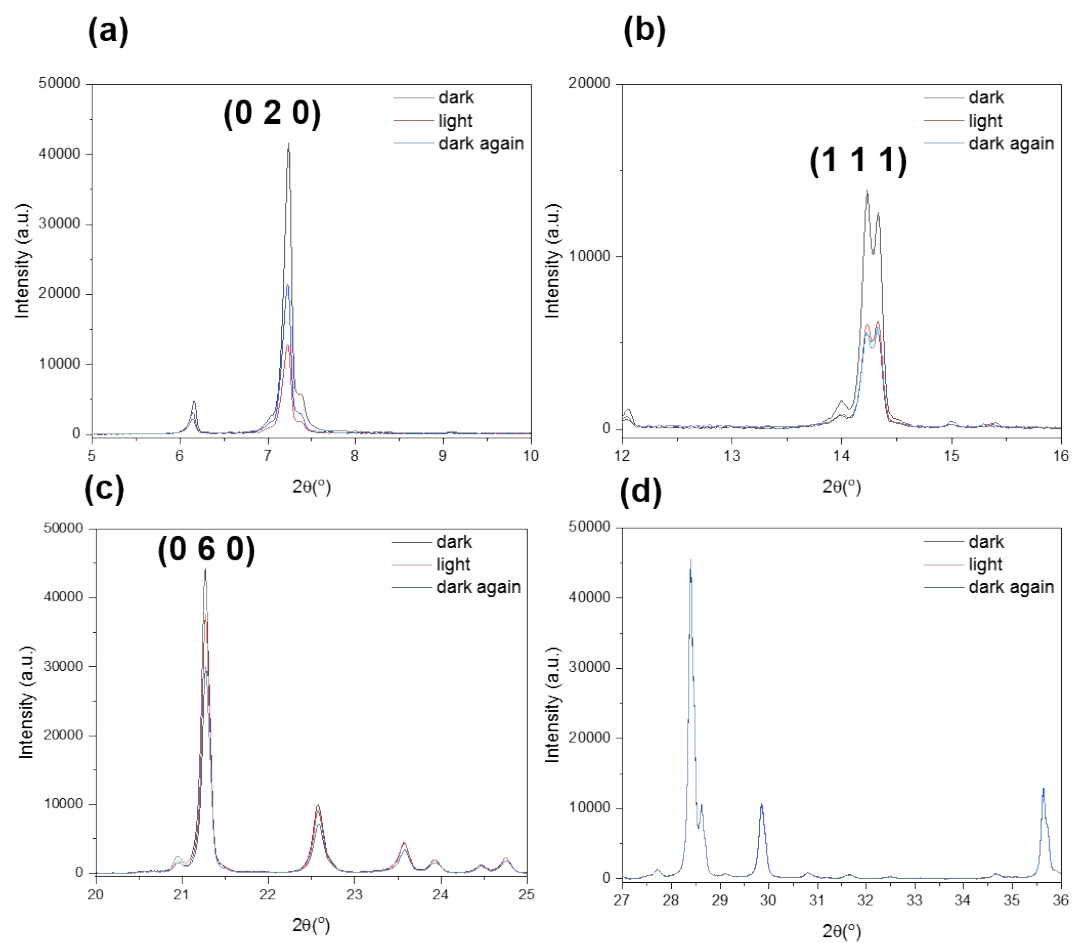


Figure S14. (a-d) Zoom-in of the peaks near 7, 14, 21, 22, 28, 30, and 36 $^\circ$ including (0 2 0), (1 1 1), (0 6 0) lattice planes in Figure 4a.

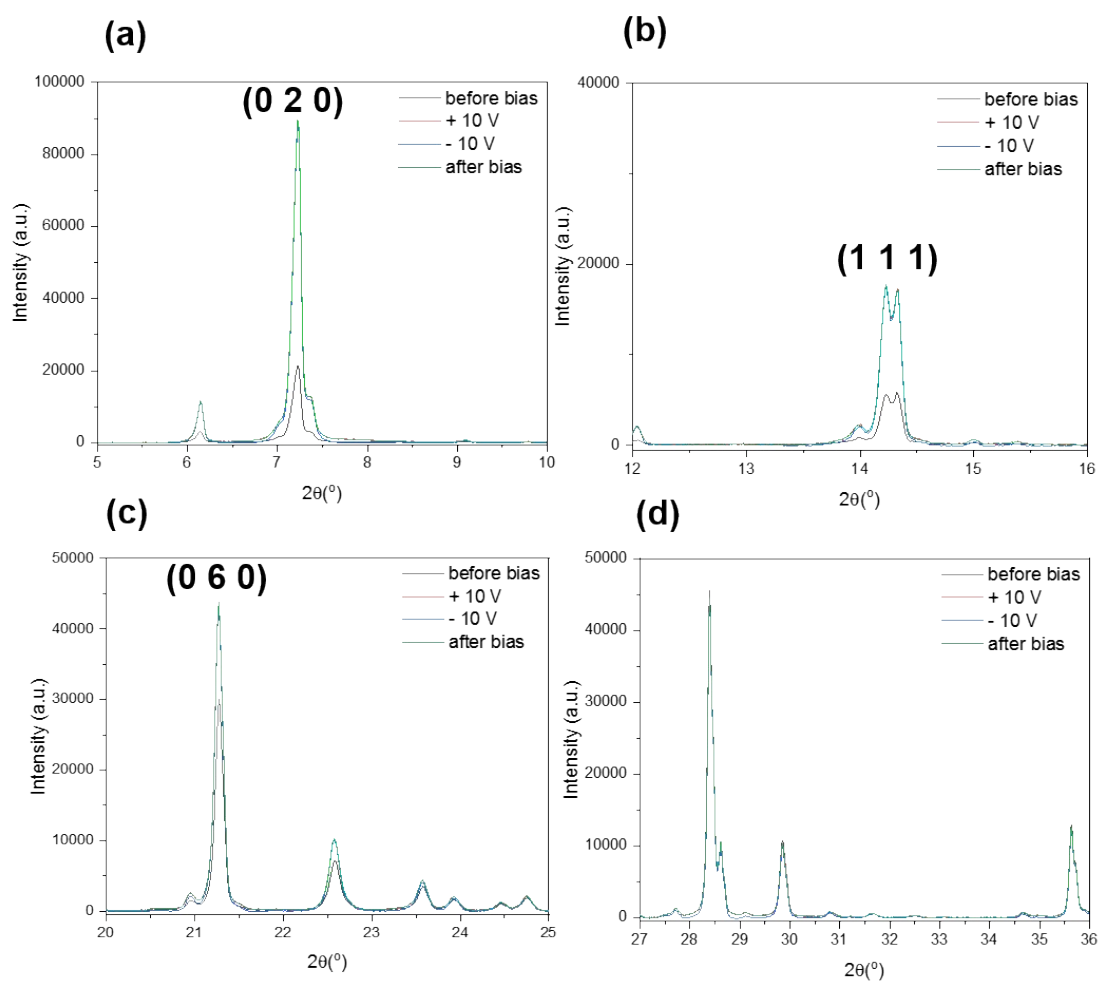


Figure S15. (a-d) Zoom-in of the peaks near 7, 14, 21, 22, 28, 30, and 36° including (0 2 0), (1 1 1), (0 6 0) lattice planes in Figure 4b.

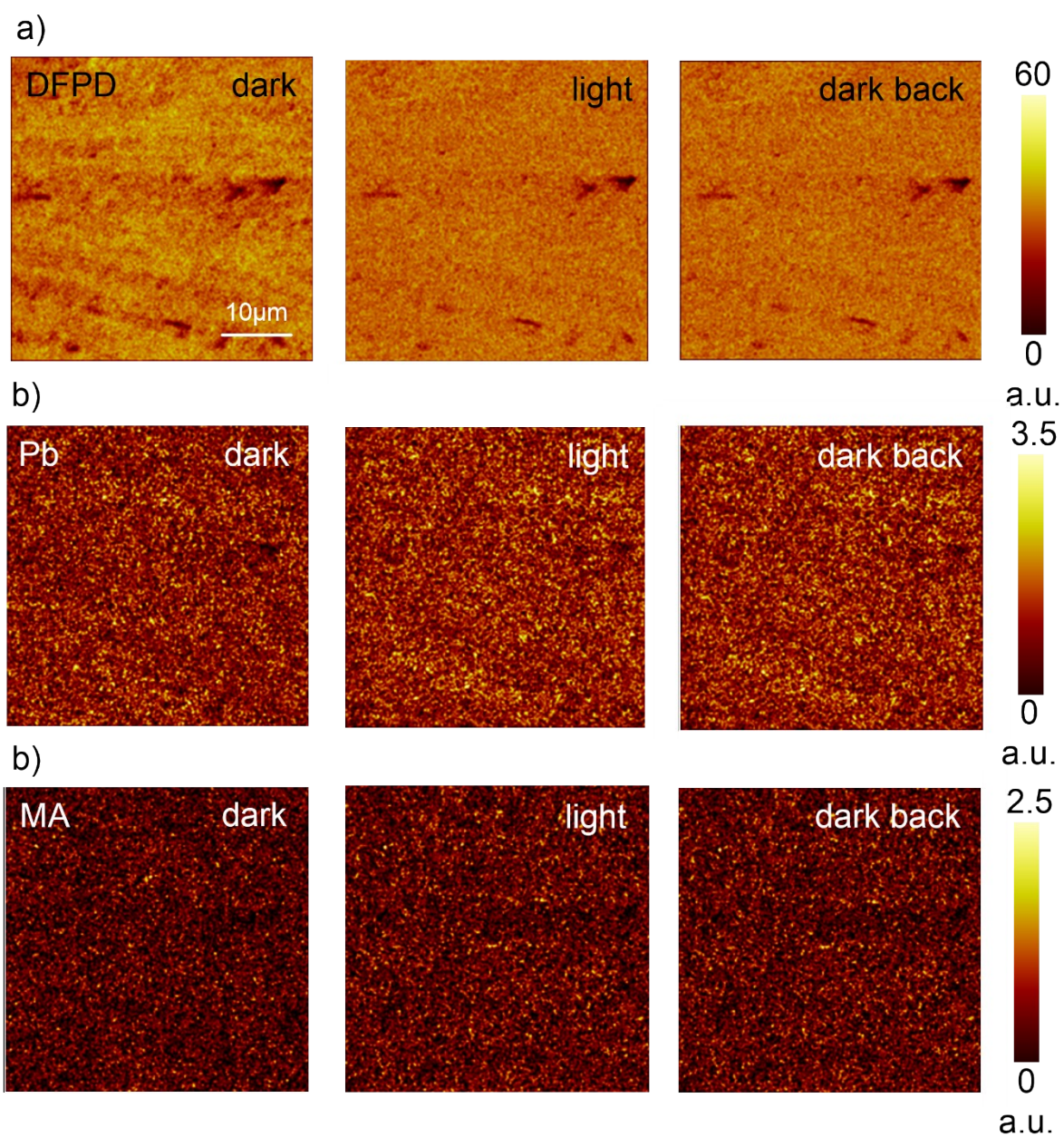


Figure S16. (a) Chemical maps of DFPD⁺, (b) Pb⁺, and (c) MA⁺ positive ions in dark, under illumination and in the dark back

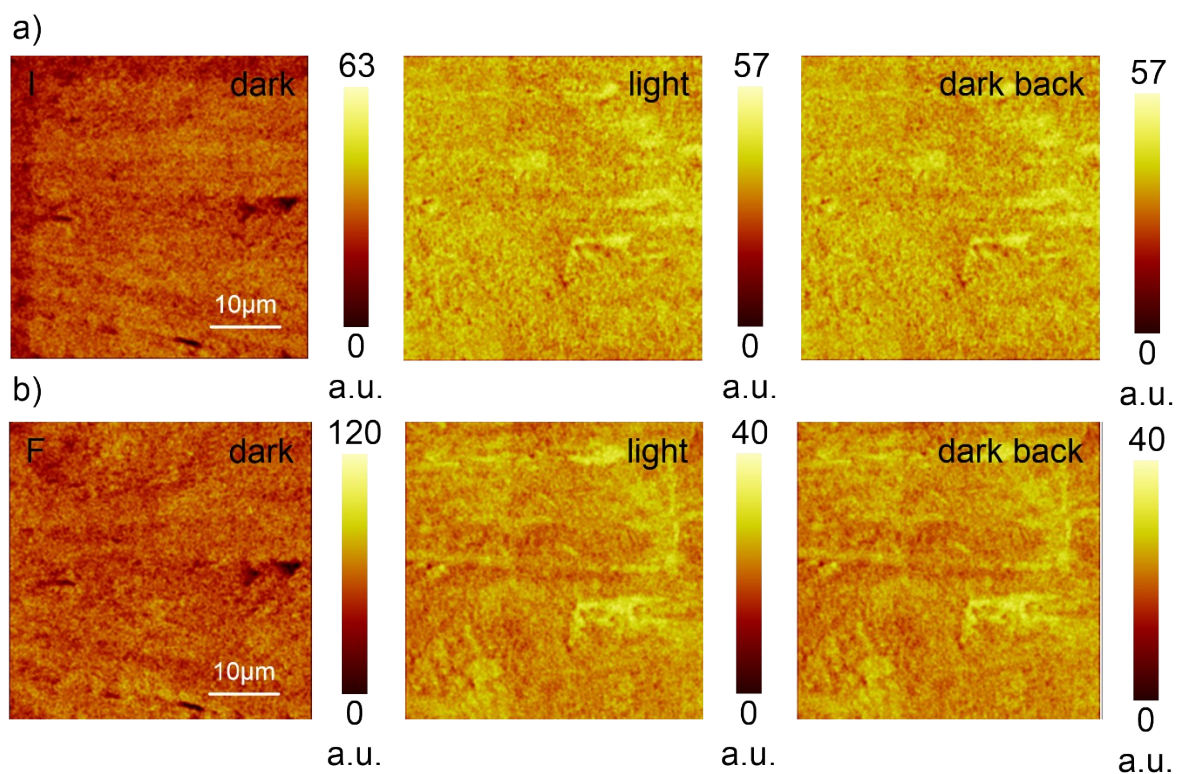


Figure S17. (a) Chemical map of I⁻ and (b) F⁻ negative ions in dark, under illumination and in the dark back

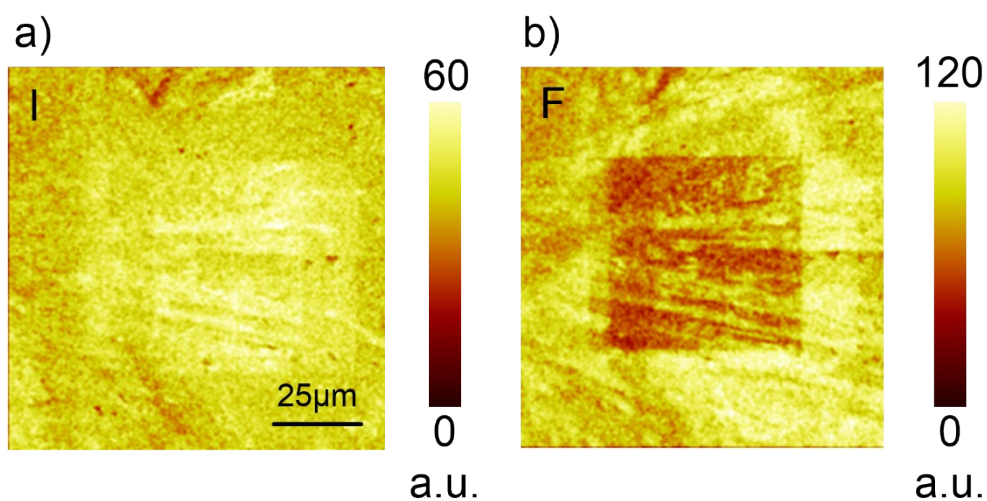


Figure S18. (a) Chemical map of I⁻ and (b) F⁻ negative ion after ToF-SIMS measurements of positive and negative modes.